

# Syngas Production via Carbon Dioxide Electroreduction Over CdS Nanorods

Jinhua Xiong<sup>1,\*</sup>, Xinyu Bi<sup>1</sup>, Song He<sup>1</sup>, Changsheng Cao<sup>2,\*</sup>

<sup>1</sup> Fujian Provincial Key Laboratory of Clean Energy Materials, Longyan University, Longyan 364000, P. R. China

<sup>2</sup> State Key Laboratory of Structural Chemistry, Fujian Institute of Research on the Structural of Matter, Chinese Academy of Science, Fuzhou 350002, China

\*E-mail: [xjh970996937@sina.com](mailto:xjh970996937@sina.com), [cscao@fjirsm.ac.cn](mailto:cscao@fjirsm.ac.cn)

Received: 7 November 2020 / Accepted: 21 December 2020 / Published: 31 January 2021

Herein, CdS nanorods (CdS-NR) was synthesized through a simple and facile solvothermal method. XRD pattern and TEM/HRTEM images indicated that hexagonal CdS nanorods with a diameter of 10 nm were successfully prepared. When used as electrocatalyst for CO<sub>2</sub> reduction reaction (CO<sub>2</sub>RR), CdS-NR afforded an excellent electrocatalytic performance in aqueous electrolyte. In comparison with commercial CdS nanoparticles (CdS-NP), CdS-NR could trigger the electroreduction of CO<sub>2</sub> to CO with a higher faradic efficiency and current densities. The enhanced electrochemical performance of CdS-NR than that of CdS-NP were ascribed to its enhanced adsorption of CO<sub>2</sub>, charge transfer ability and more exposed active sites. More importantly, it was noticed that H<sub>2</sub> generated along with CO, and the generated gas products with controllable ratios exhibited impressive potentials to directly using as syngas.

**Keywords:** CdS nanorods, electrocatalysis, CO<sub>2</sub> reduction, syngas

## 1. INTRODUCTION

Syngas, a mixture of CO and H<sub>2</sub> with certain ratios, is an indispensable feed gas for the production of important chemicals like methanol, olefin and alkane [1]. Industrially, syngas is mainly produced through gasification and natural gas reforming process, which is always an energy and cost intensive process [2]. Alternatively, syngas production via electrocatalytic CO<sub>2</sub> reduction reaction (CO<sub>2</sub>RR) in ambient conditions shows a prospectively potentials in the future [3].

Up to now, some electrocatalysts were artfully designed to produce syngas with controllable ratios of CO and H<sub>2</sub>. Wen *et al.* reported that ingenious designing of Cu nanoparticles decorated reduced graphene oxide achieved the easily production of syngas with a tuneable ratio of H<sub>2</sub>/CO from

1.16 to 6.38 [4]. Chen and his co-workers found that carefully preparation of Co/Ni single-atom catalysts with controllable ratio of Co/Ni could produce a high syngas production with CO/ H<sub>2</sub> ratios from 0.23 to 2.26 [5]. Moreover, Yang *et al.* reported that transition metal like Fe, Co and Ni decorated Au electrocatalysts was able to control the generation of H<sub>2</sub> and CO from aqueous CO<sub>2</sub>, and thus the syngas with desirable compositions was achieved [6]. Based on those results, we believe that electrocatalysts with different crystal phases, morphologies and compositions can efficiently affect the activity and selectivity for syngas production.

Recently, metal sulphides such as CuS, SnS, MoS<sub>2</sub> and In<sub>2</sub>Se<sub>3</sub> showed considerable potentials for electrocatalytic CO<sub>2</sub>RR, since their morphologies and compositions can be easily tuned [7-9]. By using ionic liquid as electrolyte, Han *et al.* reported that defective  $\gamma$ -In<sub>2</sub>Se<sub>3</sub> loaded on carbon paper delivered a current density high to 90.1 mA cm<sup>-2</sup> to produce syngas with a CO/H<sub>2</sub> ratio of 1:1 [10]. Verily recently, Gao and Yu *et al.* reported that CdS nanoneedle arrays with high-curvature nanostructure exhibited an excellent CO<sub>2</sub>RR performance with high current density and faraday efficiency for CO evolution [7]. More importantly, the crystal structure and surface state of CdS needle could be maintained during CO<sub>2</sub>RR process, which was unlike most other reported metal sulphides with unstable structure and compositions during CO<sub>2</sub>RR process. In addition, the optical and electronic properties of CdS were easily tuned via controlling exposed crystal faces of CdS [11,12]. Therefore, CdS is suitable to act as a model to study the electrocatalytic CO<sub>2</sub>RR performance of metal sulphides with different morphologies and exposed crystal faces.

In this work, CdS nanorods (CdS-NR) with preferential orientation growth along [001] were prepared by a simple solvothermal method. In comparison with commercial CdS nanoparticles (CdS-NP), the special nanorod-like morphology is beneficial for CO<sub>2</sub> adsorption, charge transfer and exposure of active sites, which is favourable to CO<sub>2</sub>RR. Correspondingly, CdS-NR shows much higher faraday efficiency and current densities for electroreduction of CO<sub>2</sub> to CO than that of CdS-NP. More significantly, syngas with CO/H<sub>2</sub> ratios from 0.33 to 1.71 can be easily obtained by precise control the applied potentials for CdS-NR. This work will shed a light on the effect of morphology and exposed crystal face of electrocatalysts on electrocatalytic CO<sub>2</sub>RR performance.

## 2. EXPERIMENT

### 2.1 Preparation of CdS nanorod (CdS-NR)

1.0 mmol CdCl<sub>2</sub>•2.5H<sub>2</sub>O was dispersed into 40 mL ethanediamine with stirring for 0.5 h. Then 4.0 mmol thiourea was added, stirring for another 0.5 h. Subsequently, the mixture was poured into a 100 mL Teflon-lined autoclave and maintained at 180 °C for 12 h. The resulting yellow solid products were centrifuged, washed with absolute ethanol and distilled water for several times, and then dried at 60 °C overnight. For comparison, CdS nanoparticle (CdS-NP) was purchased from Aladdin Co. (A. R., 98 %).

## 2.2 Characterization

The crystal structure of the as-prepared samples was examined by X-ray diffraction (XRD) patterns using a Bruker D8 Advance X-ray diffractometer with Cu K $\alpha$  radiation operated at 40 kV and 40 mA. Transmission electron microscopy (TEM) and high resolution TEM (HRTEM) images were obtained on a FEI Tecnai 20 transmission electron microscope at an accelerating voltage of 200 kV. CO<sub>2</sub> adsorption dates were recorded at ASAP 2460. All the gas products (CO and H<sub>2</sub>) were quantified with a gas chromatography (Agilent 7820A), equipped with a thermal detector and flame ionization detector. Liquid products were quantified by <sup>1</sup>H nuclear magnetic resonance spectroscopy. All the electrochemical measurements were carried out on electrochemical workstation (CHI 760)

## 2.3 Electrochemical tests

Working electrodes were prepared as following: 10 mg of CdS-NR or CdS-NP and 5 mg XC-72R carbon were dispersed in a mixture solution containing 0.7 mL H<sub>2</sub>O, 0.2 mL isopropanol and 0.1 mL 5 wt% Nafion solution with ultrasonic treatment for 2 h. Then, 0.2 mL of the catalyst ink was dropped onto the two sides of a carbon paper with a size of 1.0\*1.0 cm<sup>2</sup> and then dried at 60 °C.

All the electrochemical measurements were performed in a H-type cell separated with a proton exchange membrane (Nafion 117), in which saturated Ag/AgCl and Pt mesh were used as reference electrode and counter electrode, respectively. CO<sub>2</sub>-saturated 0.5 M KHCO<sub>3</sub> (pH  $\approx$  7.2) was used as electrolyte. CO<sub>2</sub> with a flow rate of 20.0 sccm (standard cubic centimetre per minute) was through the electrolyte during electrolysis. Linear sweep voltammetry (LSV) curves were recorded at a scan rate of 10 mV/s. The electrochemical impedance spectroscopy (EIS) was recorded at the AC amplitude of 5 mV with the frequency ranging from 0.1 Hz to 100 k Hz.

## 3. RESULTS AND DISCUSSION

### 3.1 Structure and morphology

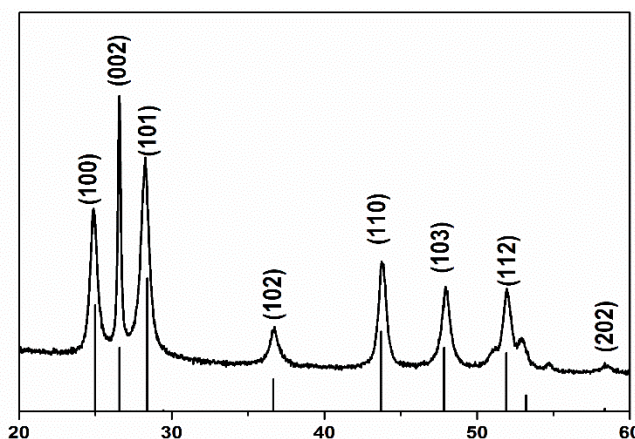
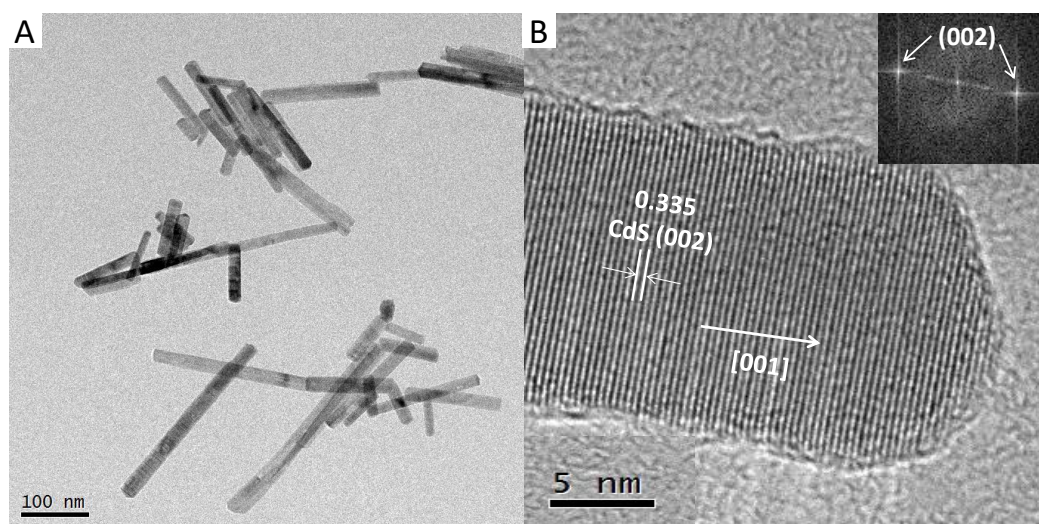


Figure 1. XRD pattern of CdS-NR.

CdS-NR was prepared via a solvothermal method. Fig. 1 showed the XRD diffraction patterns of CdS-NR. The diffraction peaks at  $2\theta$  value of 25.0, 26.6, 28.4, 36.6, 43.7, 47.8 and 51.9 ° were attributed to the (100), (002), (101), (102), (110), (103), (112) crystal planes of the hexagonal CdS (PDF#01-0780), respectively. Moreover, the microstructure of the as-prepared CdS-NR was revealed by TEM and HRTEM images. As clearly shown in Fig. 2A, CdS-NR exhibited a nanorod-like micromorphology with a diameter of 10 nm. Furthermore, the HRTEM image in Fig. 2B displayed clear crystal lattices with a spacing distance of 0.335 nm, which was ascribed to the (200) plane of hexagonal CdS [13]. In addition, the reduced fast-fourier transformed (FFT) patterns insert in Fig. 2B implied that only the diffraction characteristic of the [001] zone axis of hexagonal CdS was observed, further demonstrating the successfully synthesis of CdS nanorod.



**Figure 2.** (A) TEM and (B) HRTEM images of CdS-NR. Inset in B is the corresponding fast-fourier transformed patterns of the selected area in HRTEM.

### 3.2 Catalytic performance

Polarization curves for CdS-NR and CdS-NR were recorded with a scan rate of 10 mV/s in Ar or CO<sub>2</sub>-saturated 0.5 M KHCO<sub>3</sub>. As shown in Fig. 3A, CdS-NP and CdS-NR exhibited similar current densities under Ar atmosphere under potentials positive than -0.95V. With applied potentials become negative than -0.95 V, CdS-NP showed higher current densities. It was reported that hydrogen evolution reaction (HER)-competing reaction of CO<sub>2</sub>RR mainly happened under Ar atmosphere [14]. Therefore, it was accepted that CdS-NP and CdS-NR displayed similar HER performances in Ar-saturated electrolyte. However, in comparison with CdS-NP, CdS-NR showed much higher current densities under CO<sub>2</sub> atmosphere (Fig. 3B), demonstrating that CdS-NR possessed higher CO<sub>2</sub>RR activity [15].

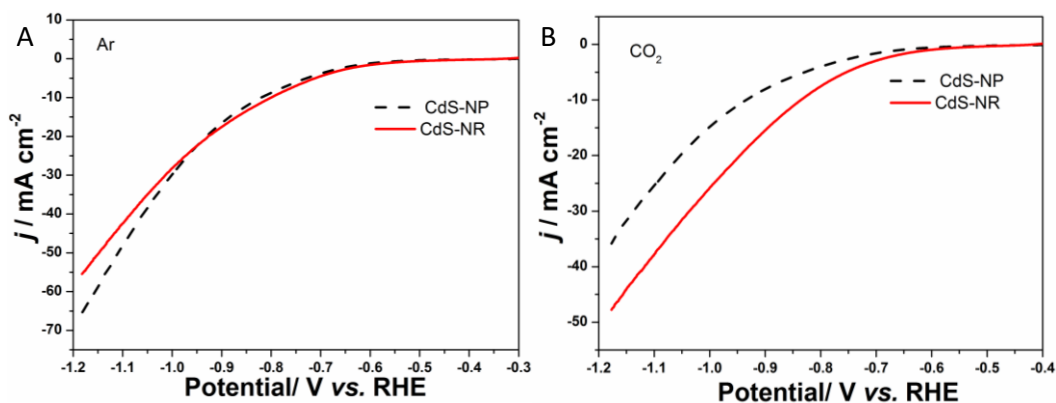


**Figure 3.** Polarization curves for CdS-NR and CdS-NP in (A) Ar or (B) CO<sub>2</sub>-saturated 0.5 M KHCO<sub>3</sub>.

The generated gaseous and liquid products for CdS-NP and CdS-NR during potentiostatic electrolysis were quantitatively measured by gas chromatography and nuclear magnetic resonance (NMR) spectra, respectively. The corresponding I-T curves for CdS-NP and CdS-NR were shown in Fig.4A and 4B, respectively. It was clearly observed that CdS-NR delivered higher current densities than that of CdS-NP under same applied potentials. According to the analysis of the generated products, CO and H<sub>2</sub> were the only detectable products under all applied potentials. As shown in Fig. 4C, the faradic efficiency (FE) of CO (FE<sub>CO</sub>) for both CdS-NP and CdS-NR increased with the applied potentials getting more negative and reached maximum at -0.978 V. However, CdS-NR displayed higher values of FE<sub>CO</sub> than that of CdS-NP under all applied potentials, and that CdS-NR possessed a maximum FE<sub>CO</sub> up to 59.6%, while it was only 44.2% for CdS-NP. Moreover, CdS-NR also showed much higher partial current densities of CO than that of CdS-NP (Fig. 4D), demonstrating that CdS-NR had a better CO<sub>2</sub>RR performance than that of CdS-NP, which is comparable to, even better than the reported CdS-based and other metal sulphides in aqueous electrolyte (Table 1) [2,7,16-21]. Meanwhile, the FEs of H<sub>2</sub> (FE<sub>H<sub>2</sub></sub>) for those two samples were shown in Fig. 4E. As observed, FEs of H<sub>2</sub> for both samples showed a same variation under different applied potentials, but FEs of H<sub>2</sub> for CdS-NP were all higher than that of CdS-NR. As well known, the tuneable ratio of CO and H<sub>2</sub> in syngas could be used to produce various chemical products. Fortunately, CO and H<sub>2</sub> were the only gaseous products in our system, which provided a platform to produce syngas with different ratio of CO and H<sub>2</sub>. As shown in Fig. 4F, CdS-NR displayed a ratio of CO/H<sub>2</sub> from 0.33 to 1.71 by changing the applied potentials. However, CdS-NP only had a narrow ratio of CO/H<sub>2</sub> from 0.18 to 0.94. The wide ratio for CO/H<sub>2</sub> made it easily to prepare specific syngas by controlling applied potentials. Hence, CdS-NR showed a perspective prospect for syngas generation.

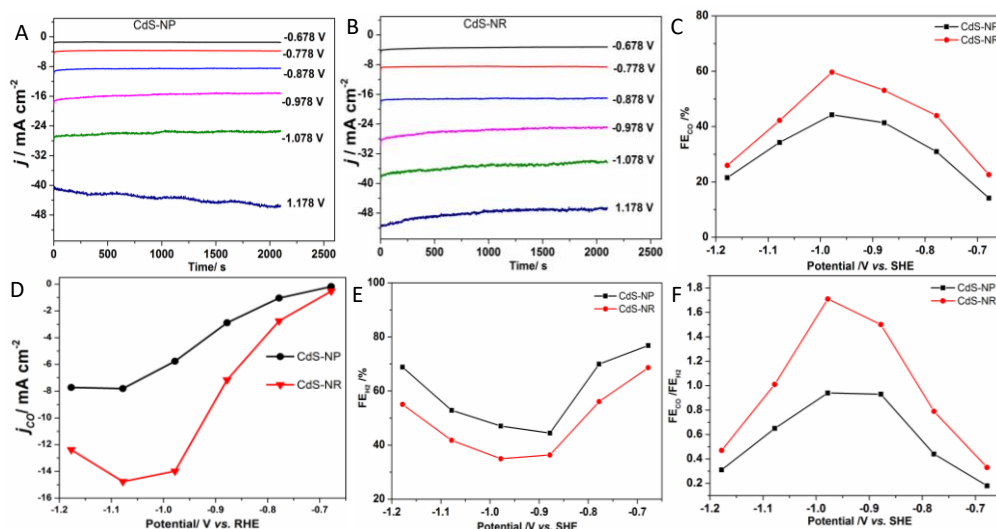


**Figure 4.** Potential-dependant I-T curves for (A) CdS-NP and (B) CdS-NR with respect of time. (C) Potential-dependent FE of CO CdS-NP and CdS-NR. (D) CO partial current densities for CdS-NP and CdS-NR. (E) Potential-dependent FE of H<sub>2</sub> for CdS-NP and CdS-NR. (F) Ratio of FE<sub>CO</sub>/FE<sub>H<sub>2</sub></sub> for CdS-NP and CdS-NR with respect of potentials.

**Table 1.** Comparison of the maximum FE<sub>CO</sub> and the corresponding CO partial current densities for CdS-NR in this work and other CdS-based and metal sulphides in aqueous electrolyte

Electrocatalyst	Electrolyte	FE <sub>CO</sub> (%)	<i>j</i> <sub>CO</sub> (mA cm <sup>-2</sup> )	Reference
CdS-NR	0.5 M KHCO <sub>3</sub>	59.6	14.8	This work
CdS-NP		44.2	7.8	
CdS NNs	0.5 M KHCO <sub>3</sub>	91.1	8.2	[7]
CdS-CNTs	0.1 M KHCO <sub>3</sub>	92.0	10.5	[16]
P-Cd S	0.25 M K <sub>2</sub> SO <sub>4</sub>	~70	~4	[17]
CdS nanorods	0.1 M KHCO <sub>3</sub>	81	21.9	[2]
CdS nanorods	0.5 M KHCO <sub>3</sub>	95	5.7	[18]
Cu <sub>2</sub> S	0.5 M KHCO <sub>3</sub>	15.8	31.6	[19]
h-CuS MCs	0.1 M KHCO <sub>3</sub>	32.7	-	[20]
rGO-PEI-MoS <sub>2</sub>	0.5 M NaHCO <sub>3</sub>	85.1	0.3	[21]

### 3.3 Mechanism for enhanced catalytic activity

Moreover, we further explored the origins of the better CO<sub>2</sub>RR performance of CdS-NR than that of CdS-NP. Well known that the adsorption of CO<sub>2</sub> was primary and important step for electrocatalytic CO<sub>2</sub>RR. Therefore, CO<sub>2</sub> adsorption measurement for CdS-NR and CdS-NP was firstly conducted. As shown in Fig. 5A, at the given relative pressure ( $P/P_0$ ) (0.002~0.995), CdS-NR showed a much higher CO<sub>2</sub> adsorption ability than that of CdS-NP. A better adsorption of reactant always led to a more excellent catalytic activity [22]. Furthermore, electron transfer was vital during electrocatalytic CO<sub>2</sub>RR process. Therefore, electrochemical impedance spectroscopy (EIS) was taken to analysis the charge-transfer behaviours. As shown in Fig. 5B, the smaller semicircle diameter of CdS-NR reflected a smaller charge-transfer resistance and more favourable charge transfer kinetics, which may due to the reason that the special rod-like micromorphology of CdS-NR could minimize the electron transport distance [23]. Additionally, the electrochemically active surface areas (ECSA) of CdS-NR and CdS-NP were obtained by calculating their double-layer capacitances ( $C_{dl}$ ), since ECSAs was in proportion to  $C_{dl}$ .  $C_{dl}$  was measured based on the CV curves at different scan rates under non-faradic region (Fig. 6A-B). As shown in Fig. 6C, the measured  $C_{dl}$  of CdS-NR was 1.484 mF cm<sup>-2</sup>, which was about 3.8 times larger than that of CdS-NP (0.395 mF cm<sup>-2</sup>), demonstrating that the CdS-NR provided more accessible active sites, which benefited CO<sub>2</sub>RR [24]. Overall, in comparison with traditional CdS nanoparticles, the unique nanorod-like structure endowed an enhanced electrocatalytic CO<sub>2</sub>RR performance of CdS-NR.

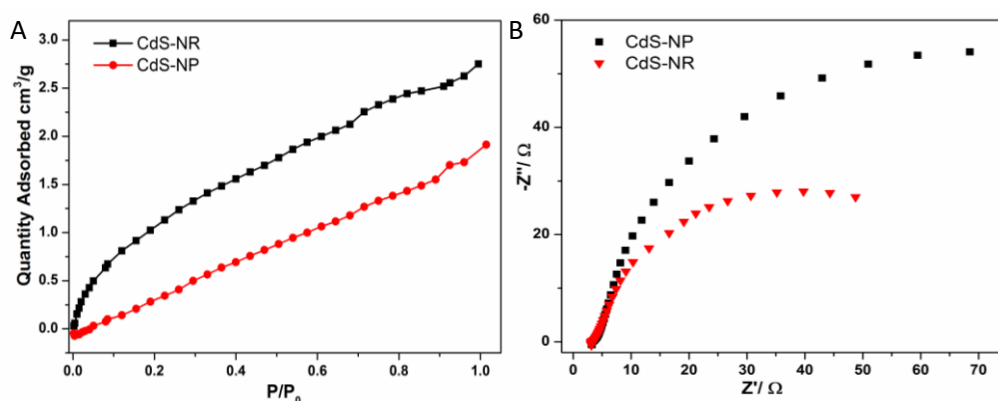


**Figure 5.** (A) CO<sub>2</sub> adsorption curves and (B) EIS for CdS-NR and CdS-NP.

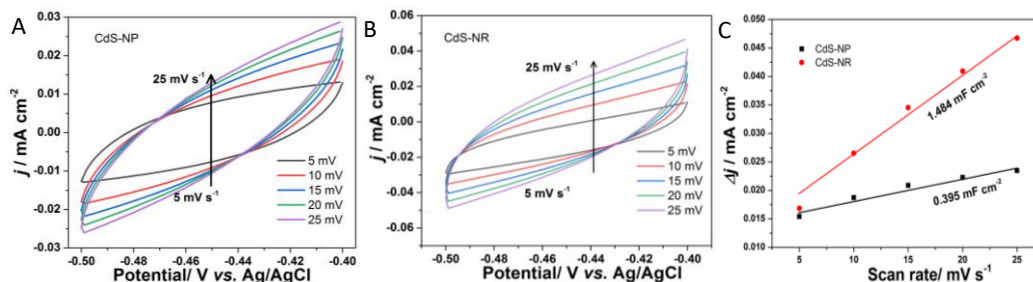


**Figure 6.** CV curves at different scan rates for (A) CdS-NP and (B) CdS-NR. (C) Capacitive  $\Delta C$  against scan rates for CdS-NP and CdS-NR.

#### 4. CONCLUSIONS

In summary, nanorod-like CdS-NR with a diameter of 10 nm was successfully synthesized via a solvothermal method, which was used as electrocatalyst to produce syngas through electrocatalytic CO<sub>2</sub> reduction reaction. In comparison with commercial CdS nanoparticles, CdS-NR exhibited a much better electrochemical performance toward syngas production in 0.5 M KHCO<sub>3</sub>. In detail, CdS-NR possessed much higher values of FE and partial current densities for CO generation. More importantly, syngas with various ratio of CO/H<sub>2</sub> from 0.33 to 1.71 could be easily obtained for CdS-NR, while CdS-NP only produces syngas with a narrow range from 0.18 to 0.94. The wide ratio for CO/H<sub>2</sub> made it desirable to prepare specific syngas by controlling applied potential. Systematic studies indicated that the special nanorod-like structure of CdS-NR was beneficial to CO<sub>2</sub> adsorption, charge transfer and exposure of more active sites, which endowed it better electrochemical performance.

#### ACKNOWLEDGEMENTS

This work was supported by Science and Technology Planning Project of Longyan (2018LYF8009), the National Natural Science Foundation of China (21802063), Natural Science Foundation of Fujian Province (2019J05116), the Doctoral Scientific Research Foundation of Longyan University (LB2018007), National Training Programs of Innovation and Entrepreneurship for Undergraduates (201811312003 and 201911312002).

#### References

1. M. B. Ross, C. T. Dinh, Y. Li, D. Kim, P. De Luna, E. H. Sargent and P. Yang, *J. Am. Chem. Soc.*, 139 (2017) 9359.
2. R. He, A. Zhang, Y. Ding, T. Kong, Q. Xiao, H. Li, Y. Liu and J. Zeng, *Adv. Mater.*, 30 (2018) 1705872.
3. S. Gao, Z. Sun, W. Liu, X. Jiao, X. Zu, Q. Hu, Y. Sun, T. Yao, W. Zhang, S. Wei and Y. Xie, *Nat. Commun.*, 8 (2017) 14503.
4. C. Cao and Z. Wen, *J. CO<sub>2</sub> Util.*, 22 (2017) 231.
5. Q. He, D. Liu, J. H. Lee, Y. Liu, Z. Xie, S. Hwang, S. Kattel, L. Song and J. G. Chen, *Angew. Chem. Int. Ed.*, 59 (2020) 3033
6. M. B. Ross, Y. Li, P. De Luna, D. Kim, E. H. Sargent and P. Yang, *Joule*, 3 (2019) 257.
7. F. Gao, S. Hu, X. Zhang, Y. Zheng, H. Wang, Z. Niu, P. Yang, R. Bao, T. Ma, Z. Dang, Y. Guan, X. Zheng, X. Zheng, J. Zhu, M. Gao and S. Yu, *Angew. Chem. Int. Ed.*, 132 (2020) 8784-8790.
8. S. N. A. Zakaria, N. Hollingsworth, H. U. Islam, A. Roffey, D. Santos-Carballal, A. Roldan, W. Bras, G. Sankar, G. Hogarth, K. B. Holt and N. H. de Leeuw, *ACS Appl. Mater. Inter.*, 10 (2018) 32078.
9. A. T. Landers, M. Fields, D. A. Torelli, J. Xiao, T. R. Hellstern, S. A. Francis, C. Tsai, J. Kibsgaard, N. S. Lewis and K. Chan, *ACS energy lett.*, 3 (2018) 1450.
10. D. Yang, Q. Zhu, X. Sun, C. Chen, W. Guo, G. Yang and B. Han, *Angew. Chem. Int. Ed.*, 132 (2020) 2374.
11. C. K. Sheng, K. A. M. A. Amin, L. L. Hong, M. F. Hassan and M. Ismail, *Int. J. Electrochem. Sci.*, 12 (2017) 10023.
12. X. He and L. Gao, *Mater. Lett.*, 63 (2009) 995.
13. J. Xiong, Y. Liu, C. Cao, L. Shen, W. Wu, S. Liang, R. Liang and L. Wu, *J. Mater. Chem. A*, 3 (2015) 6935.
14. C. Cao, D. D. Ma, J. F. Gu, X. Xie, G. Zeng, X. Li, S. G. Han, Q. L. Zhu, X. T. Wu and Q. Xu,

- Angew. Chem. Int. Ed.*, 59 (2020) 15014.
15. B. Jiang, X. G. Zhang, K. Jiang, D. Y. Wu and W. B. Cai, *J. Am. Chem. Soc.*, 140 (2018) 2880.
  16. B. Qin, Y. Li, H. Wang, G. Yang, Y. Cao, H. Yu, Q. Zhang, H. Liang and F. Peng, *Nano Energy*, 60 (2019) 43.
  17. Y. Wu, P. Zhai, S. Cao, Z. Li, B. Zhang, Y. Zhang, X. Nie, L. Sun and J. Hou, *Adv. Energy Mater.*, 10 (2020) 2002499.
  18. Y. Li, L. Cheng, P. Liu, L. Zhang, M. Zu, C. Wang, Y. Jin, X. Cao, H. Yang and C. Li, *ChemSusChem*, 11 (2018) 1421.
  19. T. Zhuang, Z. Liang, A. Seifitokaldani, Y. Li, P. D. Luna, T. Burdyny, F. Che, F. Meng, Y. Min, R. Quintero-Bermudez, C. T. Dinh, Y. Pang, M. Zhong, B. Zhang, J. Li, P. Chen, X. Zheng, H. Liang, W. Ge, B. Ye, D. Sinton, S. Yu and E. H. Sargent, *Nature Catal.*, 1 (2018) 421.
  20. P. Shao, S. Ci, L. Yi, P. Cai, P. Huang, C. Cao and Z. Wen, *ChemElectroChem*, 4 (2017) 2593.
  21. F. Li, S. Zhao, L. Chen, A. Khan, D. R. Macfarlane and J. Zhang, *Energy Environ. Sci.*, 9 (2016) 216.
  22. S. Gao, Y. Lin, X. Jiao, Y. Sun, Q. Luo, W. Zhang, D. Li, J. Yang and Y. Xie, *Nature*, 529 (2016) 68.
  23. J. Xie, J. Zhang, S. Li, F. Grote, X. Zhang, H. Zhang, R. Wang, Y. Lei, B. Pan and Y. Xie, *J. Am. Chem. Soc.*, 135 (2013) 17881.
  24. M. A. Lukowski, A. S. Daniel, C. R. English, F. Meng, A. Forticaux, R.J. Hamers and S. Jin, *Energy Environ. Sci.*, 7 (2014) 2608.